Dissipative Acousto-optic Interactions in Optical Microcavities

Jia-Wei Meng,[1,2] Shui-Jing Tang,[1,*] Jialve Sun,[3,4] Ke Shen,[1] Changhui Li,[3,5] Qihuang Gong,[1,2] and Yun-Feng Xiao[1,2,4,5,†]

[1]*Frontiers Science Center for Nano-optoelectronics and State Key Laboratory for Mesoscopic Physics, School of Physics, Peking University, Beijing 100871, China*

[2]*Collaborative Innovation Center of Extreme Optics, Shanxi University, Taiyuan 030006, China*

[3]*College of Future Technology, Peking University, Beijing 100871, China*

[4]*Peking University Yangtze Delta Institute of Optoelectronics, Nantong 226010, China*

[5]*National Biomedical Imaging Center, Peking University, Beijing 100871, China*

(Received 26 February 2022; accepted 20 July 2022; published 8 August 2022)

We propose and demonstrate experimentally the strong dissipative acousto-optic interaction between a suspended vibrating microfiber and a whispering-gallery microcavity. On the one hand, the dissipative response driven by an external stimulus of acoustic waves is found to be stronger than the dispersive response by 2 orders of magnitude. On the other hand, dead points emerge with the zero dissipative response at certain parameters, promising the potentials in physical sensing such as precise measurements of magnetic field and temperature. The strong dissipative acousto-optic interaction is then explored for ultrasensitive detection of broadband acoustic waves. A noise equivalent pressure as low as 0.81 Pa at 140 kHz in air is demonstrated experimentally, insensitive to cavity Q factors and does not rely on mechanical resonances.

DOI: 10.1103/PhysRevLett.129.073901

The interaction of optical and acoustic degrees of freedom has been widely studied in many fields, such as quantum optomechanics [1,2], acousto-optic modulation and frequency conversion [3–6], as well as acoustic sensing and imaging [7,8]. Optical microcavities can strongly enhance acousto-optic interaction by light confinement at the microscale or even nanoscale [9,10], offering new opportunities in fundamental and applied studies. For example, milestone experiments have been demonstrated such as mechanical microsolitons [11,12], single bacteria vibration [13], and chaotic mechanical breather [14]. Potentials in important applications have been recently explored in acoustic sensing [15–17], superresolution photoacoustic imaging [18–20], and high-temporal resolution atomic force microscopy [21,22].

Previous research relies mainly on the dispersive acousto-optic interaction in which acoustic waves modulate the refractive index and change the cavity geometry, resulting in the resonance shift [16–18,23–25]. A complete description of acousto-optic interaction contains dissipative terms, where acoustic waves modulate the cavity decay rate, changing the linewidth of optical modes. Nevertheless, its exploration is lagging behind compared with the dispersive interaction because the dissipative contribution is generally too weak to be observed [26–30]. Efforts have been made to enhance the dissipative coupling by utilizing mechanical resonances [29–31], in which, however, the precise control of discrete and narrow resonances relies on the delicate structures such as suspended split-beam nanocavities and spoked microdisks.

In this Letter, we report a strong dissipative acousto-optic interaction between a whispering-gallery microresonator and a suspended vibrating microfiber, driven by an external stimulus of acoustic waves. Mediated by sound-induced microfiber vibrations, the dissipative acousto-optic interaction resulting from the ultrasensitive evanescent coupling between cavity and microfiber electromagnetic modes, is observed experimentally to be stronger than the dispersive interaction by 2 orders of magnitude. The strong dissipative effect does not require mechanical resonances, and enables essentially the sensitive response to broadband acoustic waves. On the other hand, it unveils the emergence of "dead" points with the zero acoustic response at certain parameters. The "dead" points can turn to "quiet" points, which exhibit the natural resistance to acoustic disturbances, holding great potentials in precision measurements of physical quantities such as temperature, mass, and magnetic field. The dissipative acousto-optic effect is then applied to the acoustic sensing. The noise equivalent pressure (NEP) is achieved as low as 0.81 Pa at 140 kHz in air, and this detection sensitivity is demonstrated to be insensitive to cavity Q factors.

As shown in Fig. 1(a), a suspended microfiber as a mechanical element is evanescently coupled with the tightly confined whispering gallery modes of a microsphere resonator. Upon an external stimulus of acoustic waves, the optical response can occur in two ways: (i) the dispersive response. Acoustic waves alter the refractive index and cavity boundary through photoelastic effect and sound-induced

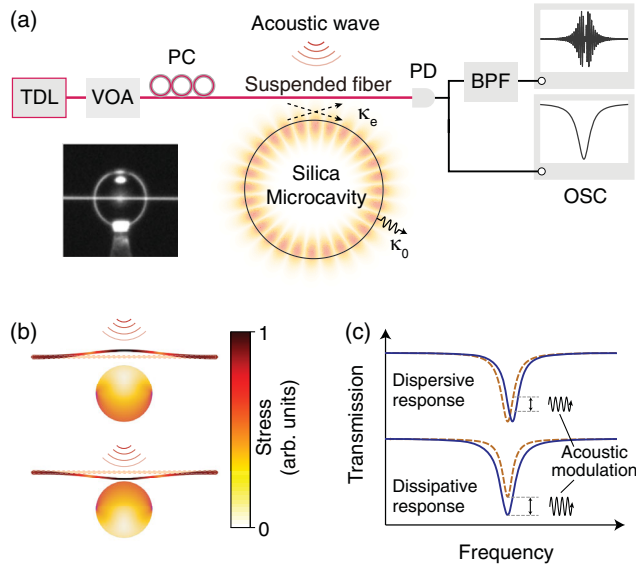

FIG. 1. (a) Schematic of the acousto-optic interaction in a microcavity-microfiber coupling system. The suspended vibrating microfiber is driven by acoustic waves for the dissipative acousto-optic interaction, modulating the coupling dissipation κ_e of cavity modes; κ_0, the intrinsic loss of the cavity mode. TDL, tunable diode laser; VOA, variable optical attenuator; PC, polarization controller; PD, photodetector; BPF, bandpass filter; OSC, oscilloscope. Inset, the optical image of the microfiber-microsphere coupling system. (b) Stress field distribution of the microfiber and microcavity as acoustic waves propagate to the coupling system, leading to their mechanical forced vibrations. (c) The dispersive and dissipative responses induced by acoustic modulations.

strains [29,32], respectively, introducing the cavity resonance shift; (ii) the dissipative response. Acoustic waves lead to the mechanical forced vibration of the suspended microfiber, altering the evanescent coupling between the cavity and fiber modes, and therefore the coupling dissipation, as shown in Fig. 1(b). Here, the vibration of the microsphere is generally negligible compared to the fiber taper [33]. Both the dispersive and dissipative responses can be translated into the intensity variation of the transmitted light [Fig. 1(c)]. Because of the rapidly decaying evanescent fields of both microresonator and microfiber, their coupling dissipation is ultrasensitive to the mechanical motions of the suspended microfiber driven by acoustic waves. Moreover, the mechanical motions actuated by sound pressures do not rely on mechanical resonances, and enable essentially the sensitive response to broadband acoustic waves.

Theoretically, when acoustic waves with frequencies ω_a drive the suspended microfiber, its forced vibration modulates the microfiber-microcavity gap distance r. In this case, the intensity variation of the transmitted light is determined by two aspects: (i) the change of coupling dissipation, which is decided by the optical evanescent field gradients of both cavity and fiber modes; (ii) the accompanied change of the transmission, which results from the dual-beam interference between the direct transmitted field of the microfiber and the intracavity field coupled back to the microfiber. Thus, the acoustic response is given by

$$S = \alpha \frac{\partial T}{\partial \kappa_e} \frac{d\kappa_e}{dr}, \tag{1}$$

where T is the normalized transmission of the microfiber, $\alpha = dr/dP(\omega_a)$ represents the mechanical sensitivity coefficient of the microfiber to acoustic waves with the pressure $P(\omega_a)$, which can be regarded as a constant here. According to the coupled-mode theory [33], $\partial T/\partial \kappa_e = 4\kappa_0(\kappa_e^2 - \kappa_0^2 - 4\Delta^2)/[(\kappa_e + \kappa_0)^2 + 4\Delta^2]^2$, with $\Delta = \omega_p - \omega_c$ being the detuning between the frequency ω_p of the probe light and the cavity resonant frequency ω_c, κ_0 the intrinsic photon decay rate of the cavity mode; κ_e the coupling dissipation of the cavity mode, which is determined by the interaction strengths between cavity modes and microfiber modes [33]. Note that this theorem is applicable for the steady-state condition with $\omega_a \ll \kappa_0$, while the acoustic response exhibits different behaviors when ω_a is comparable to or larger than the cavity decay rate $\kappa_0 + \kappa_e$ [38–40].

It is well known that the optical field gradients of evanescent fields decrease exponentially with the distance from microcavity and microfiber surfaces. The acoustic response of the coupling system is supposed to become larger with the stronger coupling strength. However, the dissipative acoustic response $|S|$ reaches the maximum at the undercoupled regime with $\kappa_e/\kappa_0 \approx 1/4$ and $\Delta = 0$, and surprisingly, the "dead" points with zero response emerge at $|\Delta| = \sqrt{\kappa_e^2 - \kappa_0^2}/2$ for $\kappa_e/\kappa_0 \geq 1$ [Figs. 2(a) and 2(b)]. These phenomena arise from the trade-off between optical field gradients and transmission variations as shown in Figs. 2(c) and 2(d), respectively. The coupling dissipation κ_e changes greatly with the smaller microcavity-microfiber gap distances r as expected, while the transmission variation depends strongly on the cavity detunings and coupling regimes. When the probe light is on resonance, the transmission for $\kappa_e > \kappa_0$ presents antiphase changes compared with that for $\kappa_e < \kappa_0$, and the zero value, corresponding to the "dead" point, emerges when $\kappa_e = \kappa_0$. As the probe light is detuned from resonance, the zero value will shift to the overcoupled regime. Note that, the "dead" points can be turned to the "quiet" points, which exhibit natural resistances to acoustic disturbances in an open environment, holding great potentials in precision measurements of physical quantities such as temperature [41,42], magnetic field [43,44], and mass [45].

Experimentally, the acoustic wave is generated by a piezoceramic stack, and its acoustic pressure can be calibrated by a hydrophone [17]. A tapered microfiber with the diameter of around 1 μm is coupled with a silica microsphere with the diameter of 70 μm and the Q factors of about 10^6. The transmission spectra are monitored by scanning the wavelength of the probe light. The acoustic

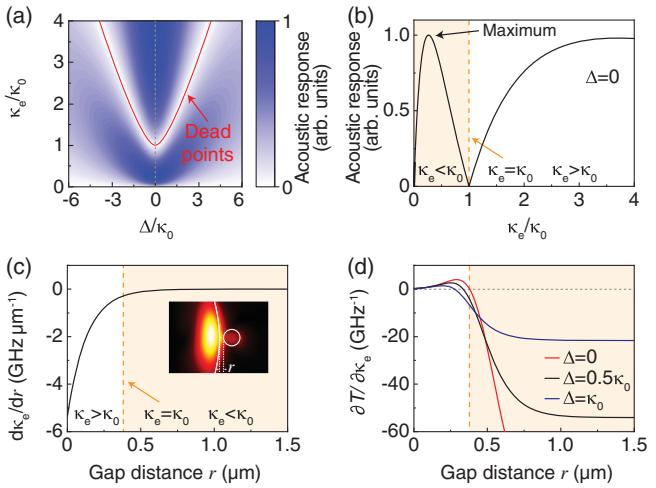

FIG. 2. (a) Dissipative acoustic response as a function of coupling dissipation κ_e and frequency detuning Δ. The dead points with the zero response are labeled with the red curve. (b) Dissipative acoustic response as a function of the coupling dissipation κ_e at $\Delta = 0$, corresponding to the response marked by the gray dashed line in (a). (c) The derivative of coupling dissipation $d\kappa_e/dr$ with different gap distance r, determined by the evanescent field gradients of fiber and cavity modes. Inset, cross-section electrical field distribution of cavity and fiber modes. (d) The partial derivative of transmission $dT/d\kappa_e$ as a function of r at different frequency detunings Δ.

responses are extracted by an electrical bandpass filter (30–800 kHz). The coupling strength between the microcavity and the microfiber is adjusted by changing their gap distance through a high-precision translation stage. The dissipative response is characterized when the microfiber is suspended with a submicrometer gap distance away from the microcavity, and the pure dispersive response is measured when the microfiber contacts with the microcavity.

The experimental results are shown in Fig. 3 with theoretical calculations. Generally, the dispersive responses induced by the acoustic modulation are independent of the coupling regimes, as presented in previous works [23,24,46]. The response vanishes on resonance ($\Delta = 0$) and reaches the maximum at the cavity detunings $|\Delta| = (\kappa_0 + \kappa_e)/2\sqrt{3}$ with the largest slope of the mode line shape [Figs. 3(a) and 3(e)]. In contrast, the dissipative responses rely on not only the cavity detuning but also the coupling regime. (i) When $\kappa_e/\kappa_0 < 1$ for the undercoupled regime, the acoustic response reaches the maximum at $\Delta = 0$ as reported previously [31], and the peak response is at $\kappa_e/\kappa_0 \approx 1/4$ for the fundamental cavity mode [Figs. 3(b) and 3(f)]. (ii) When $\kappa_e/\kappa_0 = 1$ for the critical-coupled regime, a dead point emerges with zero response at $\Delta = 0$ [Figs. 3(c) and 3(g)]. (iii) When $\kappa_e/\kappa_0 > 1$ for the overcoupled regime, the response at $\Delta = 0$ grows gradually with the larger κ_e, and the dead point splits into two branches at the cavity detunings $|\Delta| = \sqrt{\kappa_e^2 - \kappa_0^2}/2$ [Figs. 3(d) and 3(h)]. The quiet phenomenon is attributed to the reverse changes in the transmission introduced by the broadening linewidth and decreasing coupling efficiency of the cavity mode [the inset of Fig. 3(d)].

The strong dissipative acousto-optic interaction of this coupling system is then applied to ultrasensitive ultrasound detection. To this end, we detect the ultrasound wave with the frequency of 140 kHz, far away from the low-order

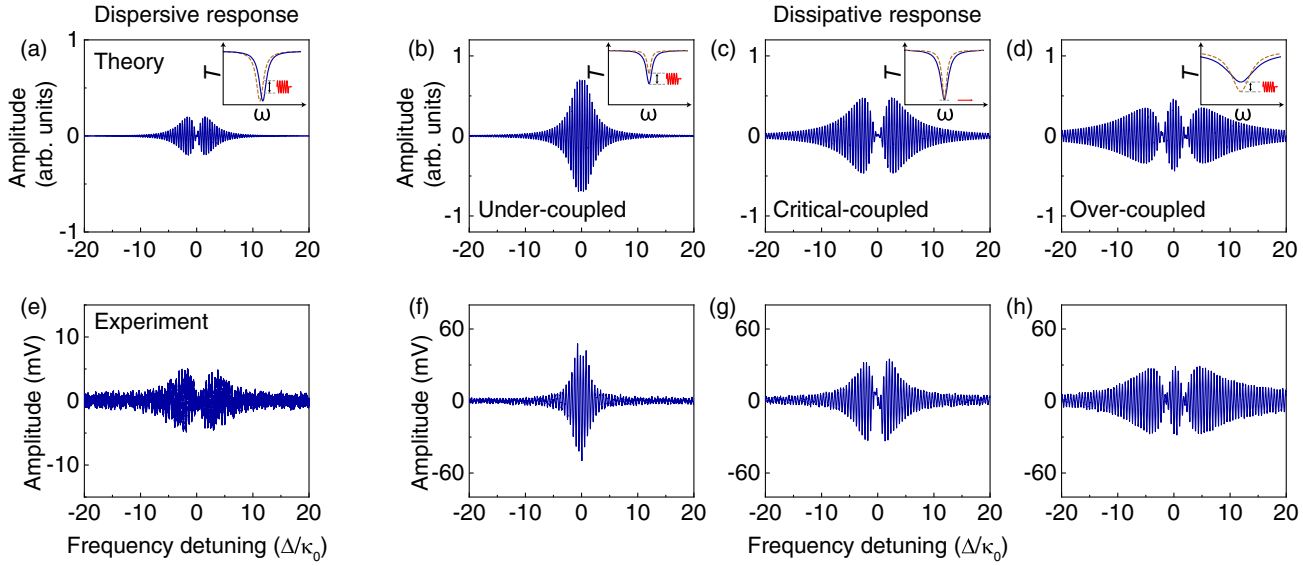

FIG. 3. Theoretical calculations (a)–(d) and experimental results (e)–(h) of acoustic responses of dispersive and dissipative interactions at the different frequency detunings Δ and coupling regimes. The frequency of acoustic waves is 140 kHz. Insets: the principles of dispersive and dissipative acousto-optic interactions [top right in (a)–(d)]. The theoretical results are calculated at a given vibration amplitude ~50 nm of the microfiber taper in (a)–(d). Coupling regimes: $\kappa_e/\kappa_0 \sim 1$ [(a), (c), (e), and (g)], $\kappa_e/\kappa_0 \sim 0.25$ [(b) and (f)], $\kappa_e/\kappa_0 \sim 2$ [(d) and (h)].

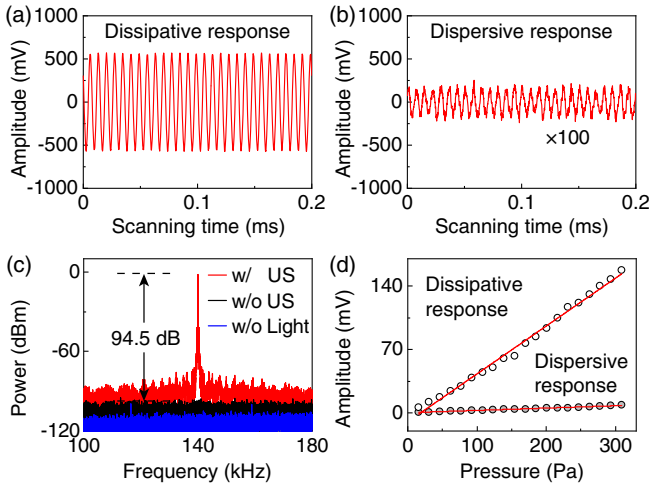

FIG. 4. (a) and (b) Intensity variation of transmitted light induced by 140-kHz ultrasound waves, under the dissipative and dispersive mechanisms, respectively. (c) Power spectral density of transmitted light with (red curve) and without (black curve) ultrasound modulation under the dissipative mechanism, and background noise floor without probe light (blue curve). (d) Dispersive and dissipative acoustic responses at different acoustic pressures. Red curves are the linear fit of experimental results. The applied acoustic pressure is 216.2 Pa [(a)–(c)]. The dissipative response is measured on the cavity resonance [(a), (c), and (d)], and the dispersive response is measured at the detuning of 55 MHz with the largest slope of the cavity line shape [(b) and (d)].

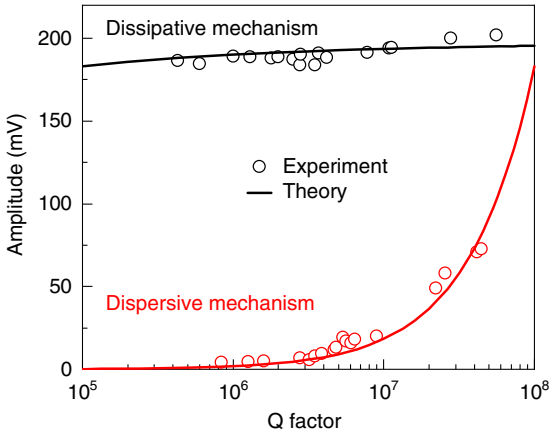

FIG. 5. Detection sensitivity at different Q factors of dissipative and dispersive mechanisms. Circles, experimental results. Curves, theoretical results.

mechanical resonance frequencies of the fiber taper [33]. The maximum acoustic response, with the applied acoustic pressure of $P(\omega_a) = 216.2$ Pa, is monitored as shown in Fig. 4(a). The dispersive response is then measured for the same cavity mode with a less than twofold decrease in the Q factor [Fig. 4(b)]. It reveals that the maximum dispersive response, determined mainly by intrinsic mechanical properties of the silica material (photoelastic coefficient and Young's modulus [32,47]), is 2 orders of magnitude smaller than the dissipative response. The NEP of the dissipative mechanism is measured as low as 0.81 Pa according to the root-mean-square noise of the transmitted light without applied ultrasound waves.

The power spectral density of the detection system is then analyzed by a spectrum analyzer with and without applied ultrasound waves in Fig. 4(c). A 94.5 dB signal-to-noise ratio ($W_{\mathrm{SNR}} = W_s/W_n$ with W_s and W_n being the measured power of the signal and noise, respectively) is observed over an integration time of $\tau = \Delta f^{-1}$, where $\Delta f = 10$ Hz is the resolution bandwidth of the spectrum analyzer. Here, the noise floor is attributed mainly to the laser shot noise and background electronic noise [48]. The NEP spectral density of this sensing system $P_{\mathrm{min}}(\omega) = 1.29\ \mathrm{mPa}/\sqrt{\mathrm{Hz}}$ limited by these fundamental noises is obtained by $P_{\mathrm{min}}(\omega_a) = \sqrt{\tau/W_{\mathrm{SNR}}} \times P(\omega_a)$ [31]. Here, the NEP spectral density is the minimum detectable acoustic pressure with $W_{\mathrm{SNR}} = 1$ in a one-hertz output bandwidth. It is determined by the voltage responsivity of the sensing system to acoustic pressure $R(\omega_a) = \sqrt{W_s}/P(\omega_a)$ and the noise power spectral density S_n without applied acoustic wave. That is, $P_{\mathrm{min}}(\omega_a) = \sqrt{S_n}/R(\omega_a)$, with $W_n = S_n \Delta f$. In addition, the intensity modulations of the transmitted light as a function of acoustic pressures are recorded to confirm the linearity of acoustic responses for ultrasound detection [Fig. 4(d)].

We then explore the detection sensitivity of the microcavity-microfiber coupling system with different Q factors. For the conventional dispersive mechanism, the intensity modulation of the transmitted light induced by the resonance shift depends linearly on the slope of mode line shape, and therefore Q factors. However, it is found that the Q-factor dependence of the dissipative mechanism is fundamentally different. Theoretically, the dissipative acoustic response in Eq. (1) at $\Delta = 0$ with the same $\eta = \kappa_e/\kappa_0$ can be simplified as $S = \alpha C (d\kappa_e/dr)/\kappa_e$, where the coefficient $C = 4\eta(\eta - 1)/(\eta + 1)^3$ is a constant. Numerically, $(d\kappa_e/dr)/\kappa_e$ remains almost unchanged and approximates $7.80 \sim 8.05$ for the $Q = \omega_c/(\kappa_0 + \kappa_e)$ ranging from 10^5 to 10^8 [33], revealing that the dissipative response is insensitive to Q factors. This behavior is then experimentally confirmed. We utilize an extra scatterer to control the intrinsic Q factor of the same cavity mode. The ultrasound responses are measured under a fixed coupling efficiency corresponding to the same $\eta = \kappa_e/\kappa_0$. As shown in Fig. 5, when the mode Q factor is reduced from 10^8 to 10^5, the detection sensitivity remains almost unchanged, while it decreases by 3 orders of magnitude for the dispersive mechanism, in good agreement with theoretical predictions.

In conclusion, we have demonstrated experimentally a strong dissipative acousto-optic interaction in a microfiber-microcavity coupling system, and unveiled its "dead" phenomenon with zero acoustic response. The strong

dissipative interaction is then applied to the ultrasensitive detection of acoustic waves, exhibiting several new characteristics. First, the detection sensitivity shows the 2-orders-of-magnitude improvement over the dispersive mechanism in the same device. Second, the detection sensitivity is demonstrated to be insensitive to mode Q factors and does not rely on the mechanical properties of cavity materials. The study of strong dissipative acousto-optic interaction can be extended to on-chip integrated microresonators using a cantilever waveguide coupler for reproducible fabrication [49]. It may find urgent applications in high-resolution photoacoustic microscopy and tomography which are challenging by using conventional optical sensors with optical fibers [16,50–54] and free-space optics [55].

We thank C.-W. Qiu for the helpful discussions. This project is supported by the National Key R&D Program of China (Grants No. 2018YFB2200401 and No. 2017YFE0104200), the National Natural Science Foundation of China (Grants No. 11825402, No. 11654003, No. 62105006, and No. 92150301), and the High-performance Computing Platform of Peking University. S.-J. T. is supported by the China Postdoctoral Science Foundation (Grants No. 2021T140023 and No. 2020M680187).

*sjtang@pku.edu.cn
†yfxiao@pku.edu.cn

[1] S. Barzanjeh, A. Xuereb, S. Gröblacher, M. Paternostro, C. A. Regal, and E. M. Weig, Optomechanics for quantum technologies, Nat. Phys. **18**, 15 (2022).
[2] W. P. Bowen and G. J. Milburn, *Quantum Optomechanics* (CRC Press, Boca Raton, 2015).
[3] C. J. Sarabalis, R. Van Laer, R. N. Patel, Y. D. Dahmani, W. Jiang, F. M. Mayor, and A. H. Safavi-Naeini, Acousto-optic modulation of a wavelength-scale waveguide, Optica **8**, 477 (2021).
[4] W. Jiang, C. J. Sarabalis, Y. D. Dahmani, R. N. Patel, F. M. Mayor, T. P. McKenna, R. Van Laer, and A. H. Safavi-Naeini, Efficient bidirectional piezo-optomechanical transduction between microwave and optical frequency, Nat. Commun. **11**, 1166 (2020).
[5] L. Shao, M. Yu, S. Maity, N. Sinclair, L. Zheng, C. Chia, A. Shams-Ansari, C. Wang, M. Zhang, K. Lai, and M. Lončar, Microwave-to-optical conversion using lithium niobate thin-film acoustic resonators, Optica **6**, 1498 (2019).
[6] E. A. Donley, T. P. Heavner, F. Levi, M. Tataw, and S. R. Jefferts, Double-pass acousto-optic modulator system, Rev. Sci. Instrum. **76**, 063112 (2005).
[7] G. Wissmeyer, M. A. Pleitez, A. Rosenthal, and V. Ntziachristos, Looking at sound: Optoacoustics with all-optical ultrasound detection, Light Sci. Appl. **7**, 53 (2018).
[8] L. V. Wang and J. Yao, A practical guide to photoacoustic tomography in the life sciences, Nat. Methods **13**, 627 (2016).
[9] M. Aspelmeyer, T. J. Kippenberg, and F. Marquardt, Cavity optomechanics, Rev. Mod. Phys. **86**, 1391 (2014).
[10] K. J. Vahala, Optical microcavities, Nature (London) **424**, 839 (2003).
[11] J. Zhang, B. Peng, S. Kim, F. Monifi, X. Jiang, Y. Li, P. Yu, L. Liu, Y.-x. Liu, A. Alù, and L. Yang, Optomechanical dissipative solitons, Nature (London) **600**, 75 (2021).
[12] Y. Hu, S. Ding, Y. Qin, J. Gu, W. Wan, M. Xiao, and X. Jiang, Generation of Optical Frequency Comb via Giant Optomechanical Oscillation, Phys. Rev. Lett. **127**, 134301 (2021).
[13] E. Gil-Santos, J. J. Ruz, O. Malvar, I. Favero, A. Lemaître, P. M. Kosaka, S. García-López, M. Calleja, and J. Tamayo, Optomechanical detection of vibration modes of a single bacterium, Nat. Nanotechnol. **15**, 469 (2020).
[14] A. W. Barnard, M. Zhang, G. S. Wiederhecker, M. Lipson, and P. L. McEuen, Real-time vibrations of a carbon nanotube, Nature (London) **566**, 89 (2019).
[15] W. J. Westerveld, M. Mahmud-Ul-Hasan, R. Shnaiderman, V. Ntziachristos, X. Rottenberg, S. Severi, and V. Rochus, Sensitive, small, broadband and scalable optomechanical ultrasound sensor in silicon photonics, Nat. Photonics **15**, 341 (2021).
[16] J. A. Guggenheim, J. Li, T. J. Allen, R. J. Colchester, S. Noimark, O. Ogunlade, I. P. Parkin, I. Papakonstantinou, A. E. Desjardins, E. Z. Zhang, and P. C. Beard, Ultrasensitive plano-concave optical microresonators for ultrasound sensing, Nat. Photonics **11**, 714 (2017).
[17] K. H. Kim, W. Luo, C. Zhang, C. Tian, L. J. Guo, X. Wang, and X. Fan, Air-coupled ultrasound detection using capillary-based optical ring resonators, Sci. Rep. **7**, 109 (2017).
[18] R. Shnaiderman, G. Wissmeyer, O. Ülgen, Q. Mustafa, A. Chmyrov, and V. Ntziachristos, A submicrometre silicon-on-insulator resonator for ultrasound detection, Nature (London) **585**, 372 (2020).
[19] B. Dong, H. Li, Z. Zhang, K. Zhang, S. Chen, C. Sun, and H. F. Zhang, Isometric multimodal photoacoustic microscopy based on optically transparent micro-ring ultrasonic detection, Optica **2**, 169 (2015).
[20] H. Li, B. Dong, X. Zhang, X. Shu, X. Chen, R. Hai, D. A. Czaplewski, H. F. Zhang, and C. Sun, Disposable ultrasound-sensing chronic cranial window by soft nanoimprinting lithography, Nat. Commun. **10**, 4277 (2019).
[21] L. Schwab, P. Allain, N. Mauran, X. Dollat, L. Mazenq, D. Lagrange, M. Gély, S. Hentz, G. Jourdan, I. Favero, and B. Legrand, Very-high-frequency probes for atomic force microscopy with silicon optomechanics, Microsyst. Nanoeng. **8**, 32 (2022).
[22] Y. Liu, H. Miao, V. Aksyuk, and K. Srinivasan, Wide cantilever stiffness range cavity optomechanical sensors for atomic force microscopy, Opt. Express **20**, 18268 (2012).
[23] J. Sun, J.-W. Meng, S.-J. Tang, and C. Li, An encapsulated optical microsphere sensor for ultrasound detection and photoacoustic imaging, Sci. China Phys. Mech. Astron. **65**, 1 (2022).
[24] C. Zhang, S.-L. Chen, T. Ling, and L. J. Guo, Review of imprinted polymer microrings as ultrasound detectors: Design, fabrication, and characterization, IEEE Sens. J. **15**, 3241 (2015).
[25] G. Anetsberger, O. Arcizet, Q. P. Unterreithmeier, R. Rivière, A. Schliesser, E. M. Weig, J. P. Kotthaus, and T. J. Kippenberg, Near-field cavity optomechanics with nanomechanical oscillators, Nat. Phys. **5**, 909 (2009).

[26] A. K. Tagantsev and E. S. Polzik, Dissipative optomechanical coupling with a membrane outside of an optical cavity, Phys. Rev. A **103**, 063503 (2021).
[27] A. Xuereb, R. Schnabel, and K. Hammerer, Dissipative Optomechanics in a Michelson-Sagnac Interferometer, Phys. Rev. Lett. **107**, 213604 (2011).
[28] J. Baraillon, B. Taurel, P. Labeye, and L. Duraffourg, Linear analytical approach to dispersive, external dissipative, and intrinsic dissipative couplings in optomechanical systems, Phys. Rev. A **102**, 033509 (2020).
[29] A. G. Primo, N. C. Carvalho, C. M. Kersul, N. C. Frateschi, G. S. Wiederhecker, and Thiago P. Mayer Alegre, Quasi-normal-Mode Perturbation Theory for Dissipative and Dispersive Optomechanics, Phys. Rev. Lett. **125**, 233601 (2020).
[30] M. Wu, A. C. Hryciw, C. Healey, D. P. Lake, H. Jayakumar, M. R. Freeman, J. P. Davis, and P. E. Barclay, Dissipative and Dispersive Optomechanics in a Nanocavity Torque Sensor, Phys. Rev. X **4**, 021052 (2014).
[31] S. Basiri-Esfahani, A. Armin, S. Forstner, and W. P. Bowen, Precision ultrasound sensing on a chip, Nat. Commun. **10**, 132 (2019).
[32] K. C. Balram, M. Davanço, J. Y. Lim, J. D. Song, and K. Srinivasan, Moving boundary and photoelastic coupling in GaAs optomechanical resonators, Optica **1**, 414 (2014).
[33] See Supplemental Material at http://link.aps.org/supplemental/10.1103/PhysRevLett.129.073901 for details, which includes Refs. [34–37].
[34] M. L. Gorodetsky and V. S. Ilchenko, Optical microsphere resonators: Optimal coupling to high-q whispering-gallery modes, J. Opt. Soc. Am. B **16**, 147 (1999).
[35] M. J. Humphrey, E. Dale, A. Rosenberger, and D. Bandy, Calculation of optimal fiber radius and whispering-gallery mode spectra for a fiber-coupled microsphere, Opt. Commun. **271**, 124 (2007).
[36] B. E. Little, S. T. Chu, H. A. Haus, J. Foresi, and J.-P. Laine, Microring resonator channel dropping filters, J. Lightwave Technol. **15**, 998 (1997).
[37] B. E. Little, J.-P. Laine, and H. A. Haus, Analytic theory of coupling from tapered fibers and half-blocks into microsphere resonators, J. Lightwave Technol. **17**, 704 (1999).
[38] W. D. Sacher and J. K. Poon, Dynamics of microring resonator modulators, Opt. Express **16**, 15741 (2008).
[39] K. Kalli and D. A. Jackson, Analysis of the dynamic response of a ring resonator to a time-varying input signal, Opt. Lett. **18**, 465 (1993).
[40] H. A. Haus and W. Huang, Coupled-mode theory, Proc. IEEE **79**, 1505 (1991).
[41] J. Liao and L. Yang, Optical whispering-gallery mode barcodes for high-precision and wide-range temperature measurements, Light Sci. Appl. **10**, 32 (2021).
[42] X. Jiang and L. Yang, Optothermal dynamics in whispering-gallery microresonators, Light Sci. Appl. **9**, 24 (2020).
[43] S. Forstner, S. Prams, J. Knittel, E. D. Van Ooijen, J. D. Swaim, G. I. Harris, A. Szorkovszky, W. P. Bowen, and H. Rubinsztein-Dunlop, Cavity Optomechanical Magnetometer, Phys. Rev. Lett. **108**, 120801 (2012).
[44] B.-B. Li, J. Bilek, U. B. Hoff, L. S. Madsen, S. Forstner, V. Prakash, C. Schäfermeier, T. Gehring, W. P. Bowen, and U. L. Andersen, Quantum enhanced optomechanical magnetometry, Optica **5**, 850 (2018).
[45] W. Yu, W. C. Jiang, Q. Lin, and T. Lu, Cavity optomechanical spring sensing of single molecules, Nat. Commun. **7**, 1 (2016).
[46] H. Li, B. Dong, Z. Zhang, H. F. Zhang, and C. Sun, A transparent broadband ultrasonic detector based on an optical micro-ring resonator for photoacoustic microscopy, Sci. Rep. **4**, 1 (2014).
[47] B. E. Saleh and M. C. Teich, *Fundamentals of Photonics* (John Wiley & Sons, New York, 2019).
[48] M. Jin, S.-J. Tang, J.-H. Chen, X.-C. Yu, H. Shu, Y. Tao, A. K. Chen, Q. Gong, X. Wang, and Y.-F. Xiao, $1/f$-noise-free optical sensing with an integrated heterodyne interferometer, Nat. Commun. **12**, 1973 (2021).
[49] B. Fischer, Optical microphone hears ultrasound, Nat. Photonics **10**, 356 (2016).
[50] E. Carome and K. Koo, Multimode coupled waveguide acoustic sensors, Opt. Lett. **5**, 359 (1980).
[51] G. Wild and S. Hinckley, Acousto-ultrasonic optical fiber sensors: Overview and state-of-the-art, IEEE Sens. J. **8**, 1184 (2008).
[52] A. Rosenthal, S. Kellnberger, D. Bozhko, A. Chekkoury, M. Omar, D. Razansky, and V. Ntziachristos, Sensitive interferometric detection of ultrasound for minimally invasive clinical imaging applications, Laser Photonics Rev. **8**, 450 (2014).
[53] G. Wissmeyer, D. Soliman, R. Shnaiderman, A. Rosenthal, and V. Ntziachristos, All-optical optoacoustic microscope based on wideband pulse interferometry, Opt. Lett. **41**, 1953 (2016).
[54] R. Shnaiderman, G. Wissmeyer, M. Seeger, D. Soliman, H. Estrada, D. Razansky, A. Rosenthal, and V. Ntziachristos, Fiber interferometer for hybrid optical and optoacoustic intravital microscopy, Optica **4**, 1180 (2017).
[55] A. P. Jathoul, J. Laufer, O. Ogunlade, B. Treeby, B. Cox, E. Zhang, P. Johnson, A. R. Pizzey, B. Philip, T. Marafioti *et al.*, Deep in vivo photoacoustic imaging of mammalian tissues using a tyrosinase-based genetic reporter, Nat. Photonics **9**, 239 (2015).